JOURNAL OF AGRICULTURAL AND FOOD CHEMISTRY

Using Synchrotron Transmission FTIR Microspectroscopy as a Rapid, Direct, and Nondestructive Analytical Technique To Reveal Molecular Microstructural−Chemical Features within Tissue in Grain Barley

PEIQIANG YU,† JOHN J. MCKINNON,*,† COLLEEN R. CHRISTENSEN,§ AND DAVID A. CHRISTENSEN†

College of Agriculture, University of Saskatchewan, 51 Campus Drive, Saskatoon, Saskatchewan S7N 5A8, Canada; Canadian Light Source, 101 Perimeter Road, Saskatoon, Saskatchewan S7N 0X4, Canada; Western College of Veterinary Medicine, University of Saskatchewan, 52 Campus Drive, Saskatoon, Saskatchewan S7N 5B4, Canada; and BioSynch Inc., 1305 10th Street, Saskatoon, Saskatchewan S7H 0J2, Canada

The objective of this study was to use synchrotron transmission FTIR microspectroscopy as a rapid, direct, and nondestructive analytical technique to reveal molecular microstructural−chemical features within tissue in grain barley. The results showed that synchrotron transmission FTIR microspectroscopy could provide spectral, chemical, and functional group characteristics of grain barley tissue at ultrahigh spatial resolutions. The spatially localized structural−chemical distributions of biological components (lignin, cellulose, protein, lipid, and carbohydrates) and biological component ratios could be imaged. Such information on molecular microstructural−chemical features within the tissue can be used for plant breeding programs for selecting superior varieties of barley for special purposes and for prediction of grain barley quality and nutritive value for humans and animals.

KEYWORDS: Synchrotron; transmission infrared microspectroscopy; localized chemical analysis and imaging; molecular microstructure; barley tissue

INTRODUCTION

Recently, synchrotron vibrational microspectroscopy has been developed to reveal molecular microstructural features within tissue in a variety of materials (*1*). This technique, taking advantage of synchrotron light brightness (which is usually 100−1000 times brighter than a conventional globar source and has a small effective source size), is capable of exploring the molecular chemistry within microstructures of biological samples with high signal-to-noise ratios at ultrahigh spatial resolutions as fine as 3−10 μm (*1*−*7*).

Standard globar-sourced FTIR−microspectroscopy cannot reveal chemical features of micro-biomaterials, which are <35−100 μm (depending on the type of FTIR microspectrometer). The normal plant cell size is ∼5−30 μm. With a globar source, a very poor signal-to-noise ratio within plant cellular dimensions is obtained. Synchrotron light is extremely bright, nondivergent light and the beam is intense and fine. Using synchrotron-based FTIR microspectroscopy allows a very small area to be explored, provides higher accuracy and precision, allows faster data collection, reaches diffraction limits as small as a few micrometers, and provides very good signal-to-noise ratios (S/N) with ultrahigh spatial resolutions. It can reveal plant structural chemical features within cellular dimensions (<30 μm) (*7*).

It is well-known that the total energy of a molecule consists of translational, rotational, vibrational, and electronic energies. Different radiation of the electromagnetic (EM) spectrum will result in different energy transitions in a molecule. Organic molecules possess bonds and functional groups. These functional groups vibrate independently of each other and weakly interact. Without any EM radiation effect, these molecules (functional groups) vibrate independently at their equilibrium position. However, when IR radiation (which is part of the EM spectrum) is applied to organic molecules (functional groups), it breaks down the molecule's equilibrium (position) stage, causing two energy transitions in a molecule. It promotes transitions in a molecule between rotational and vibrational energy. When transitions between rotational and vibrational energy levels occur that cause a net change in the dipole moment, the molecule will absorb IR. Therefore, an IR absorption profile is unique to a specific molecular vibration frequency. When IR radiation passes through a sample, some of it is absorbed by the sample and some of it is passed through (transmitted). The resulting spectrum represents the molecular absorption/transmission, which creates a molecular fingerprint of the sample. Identifica-

* Corresponding author [telephone (306) 966-4137; e-mail mckinnon@sask.usask.ca].
† College of Agriculture, University of Saskatchewan.
§ Canadian Light Source; Western College of Veterinary Medicine, University of Saskatchewan; and BioSynch, Inc.

10.1021/jf035065a CCC: $27.50
Published on Web 02/21/2004

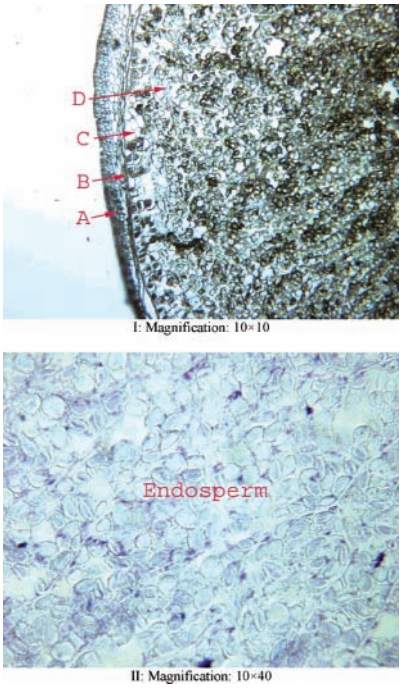

Figure 1. (Top) Photomicrograph of grain barley tissue cross section showing the inherent structure: (**A**) pericarp; (**B**) seed coat; (**C**) aleurone; (**D**) endosperm. (Bottom) Starch granules.

tion of molecular functional groups is a major application of IR spectrometry (*7*−*12*).

Because each biological component has unique molecular−chemical−structural features, each has its own unique IR spectrum. For example, the characteristic of protein is unique in the peptide bond. The peptide bond contains C═O, C−N, and N−H. The amide I bond is primarily C═O stretching vibration (80%) plus C−N stretching vibration. Amide I absorbs at ∼1650 cm^{-1}. Amide II, which absorbs at 1550 cm^{-1}, consists of N−H bending vibrations (60%) coupled with C−N stretching vibrations (40%). Lipid contains both carbonyl C═O ester as well as CH_2 and CH_3 functional groups. The unique IR spectral profile for lipid is at ca. 1738 cm^{-1} (carbonyl C═O), 1470 cm^{-1} (CH bending), 2961 cm^{-1} (asymmetric stretch CH_3), 2925 cm^{-1} (asymmetric stretch CH_2), 2871 cm^{-1} (symmetric stretch CH_3), and 2853 cm^{-1} (symmetric stretch CH_2), (*12*). Carbohydrates have lots of sugars and lots of OH and CO bonds. Depending on bond linkage and type of sugar, the IR position for carbohydrate is between 1180 and 950 cm^{-1}. The same principle applies to other biological components, such as lignin at 1510 cm^{-1}, hemicellulose at 1246 cm^{-1}, cellulose at 1100 cm^{-1}, and starch at 1025 cm^{-1} (*1*−*6*, *13*, *14*).

The research on nutritive values of barley varieties has been of interest in our laboratory (*15*, *16*). The objective of this study was to use synchrotron transmission FTIR microspectroscopy as a rapid, direct, and nondestructive analytical technique to

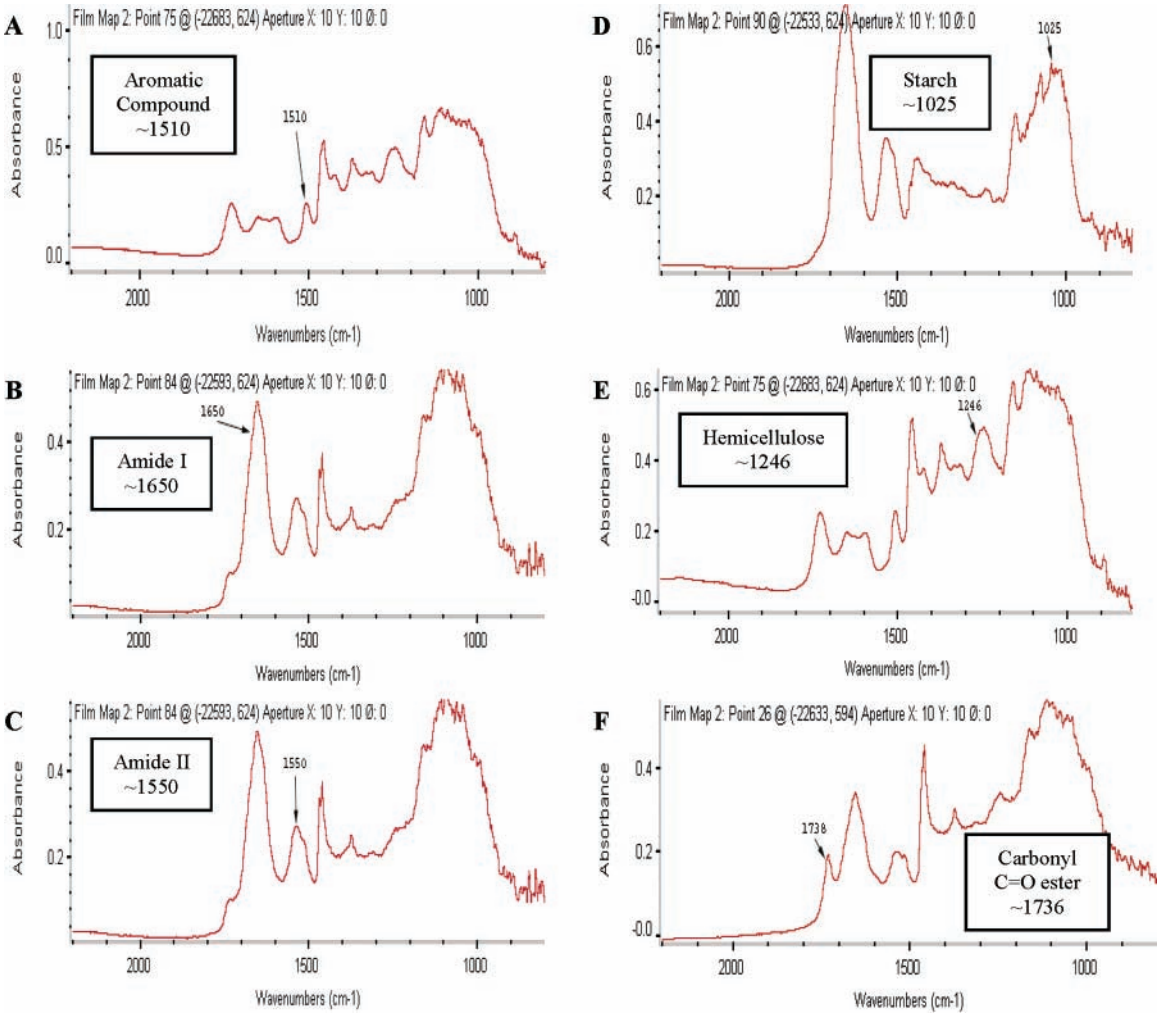

Figure 2. Synchrotron mid-IR fingerprint bands for aromatic compounds (lignin) (**A**), amide I (**B**), amide II (**C**), carbohydrates including nonstructural carbohydrate (starch) (**D**) and structural carbohydrate (hemicellulose) (**E**), and carbonyl C═O ester (**F**) in barley tissue.

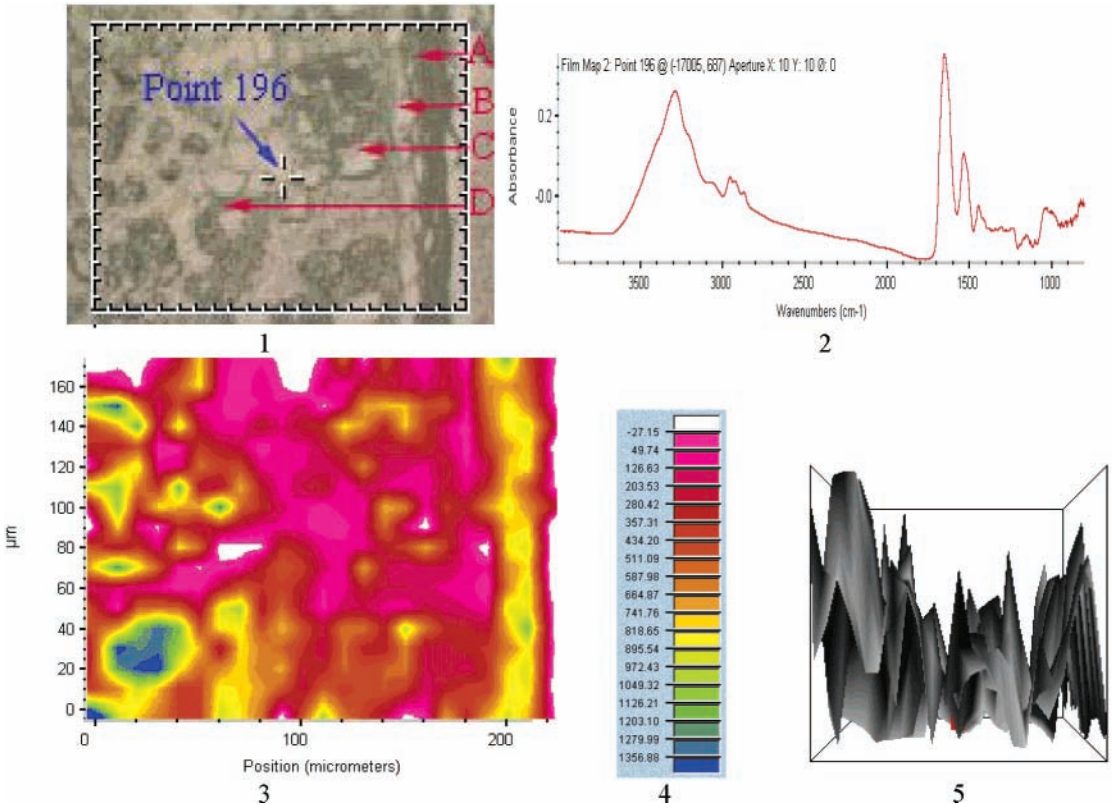

Figure 3. Area under 4000–800 cm^{-1} peak showing mid-IR total functional group intensity: (**1**) visible image [(**A**) pericarp; (**B**) seed coat; (**C**) aleurone; (**D**) endosperm region]; (**2**) spectrum corresponding to the pixel at the cross hair in the visible image; (**3**) chemical image; (**4**) chemical intensity ruler; (**5**) 3D image.

reveal molecular microstructural−chemical features within tissue in grain barley designated for animal feed.

MATERIALS AND METHODS

Grain Barley. Grain barley (feed type, Valier) was grown in a university research plot near Saskatoon (Canada). The barley samples were supplied by Crop Development Center (CDC), University of Saskatchewan (Saskatoon, SK, Canada).

Transmission FTIR Microspectroscopic Window Preparation. The barley samples were frozen at −20 °C on objective disks with paraffin as embedding material in a microtome (Tissue Tech) and then cut into thin cross sections (~6 μm thickness) using a microtome and paraffin was removed using xylene at Western College of Veterinary Medicine, University of Saskatchewan, Canada. The cross sections of the tissues were rapidly transferred to BaF_2 windows (size = 13 × 1 mm disk; part 915-3015, Spectral Systems) for use in synchrotron transmission FTIR microspectroscopic work.

Photomicrograph of Cross Sections of Plant Tissue. Photomicrographs (10 × 10 and 10 × 40 magnification) of cross sections of the barley tissue (thickness = ~6 μm) were taken by an Olympus microscope (Olympus BH-2) with digital camera from regular glass slides.

Synchrotron Light Source and Transmission FTIR microspectroscopy. This experiment was performed at the National Synchrotron Light Source in Brookhaven National Laboratory, U.S. Department of Energy (NSLS-BNL, Upton, NY). The spectroscopic images were recorded using a Nicolet Magna 860 FTIR (Thermo Nicolet) equipped with a Continuμm IR microscope (Spectra Tech), a mapping stage controller, a 32× objective, and a mercury cadmium telluride (MCT-A) detector. The bench was configured with a synchrotron light beamline with an energy level of 800 MeV (U10B, NSLS-BNL). The spectra were collected in the mid-infrared range of 4000−800 cm^{-1} at a resolution of 4 cm^{-1} with 64 scans co-added and an aperture setting of ca. 10 × 10 μm. A background spectroscopic image file was collected from an area free of sample. The mapping steps were equal to aperture size. Scanned visible images were obtained using a charge-coupled device (CCD) camera linked to the infrared images.

Data Analysis and Chemical Imaging. The spectral data of the barley tissues were collected, corrected with the background spectrum, displayed in the absorbance mode, and analyzed using OMNIC software 6.0 (Spectra Tech). The data can be displayed either as a series of spectroscopic images collected at individual wavelengths or as a collection of infrared spectra obtained at each pixel position in the image. Chemical imaging of functional groups was determined by the OMNIC software 6.0 (Spectra Tech): protein indicated by amide I or II, lipid indicated by carbonyl C═O ester linkage band, total carbohydrates, lignin, hemicellusoic and cellulosic materials were determined by the OMNIC software 6.0 (Spectra Tech) (*2*, *6*, *13*). Peak height or area ratio images were obtained by the height or area under one functional group band (such as amide I, 1650 cm^{-1}) divided by the height or area under another functional group band (such as starch, 1025 cm^{-1}) at each pixel (pixel size 10 × 10 μm), which represents the biological component ratio intensity and distribution in the tissue (e.g., protein to total starch ratio image and hemicellulose to total carbohydrate ratio image).

RESULTS AND DISCUSSION

Photomicrograph of Grain Barley Tissue. The inherent structures of the barley tissue are illustrated in **Figure 1**. The photomicrographs show barley structure from the pericarp at the outside of the seed, to the seed coat, through to the aleurone layer and the endosperm. The pericarp forms the tough outer covering of the seed kernel and provides protection for the interior components. The seed coat is found between the pericarp and the aleurone layer. The aleurone cells play an important role during seedling development. The endosperm (**Figure 1**) consists of cells filled mainly with starch granules. However, such photomicrographs do not give information on localized structural−chemical information.

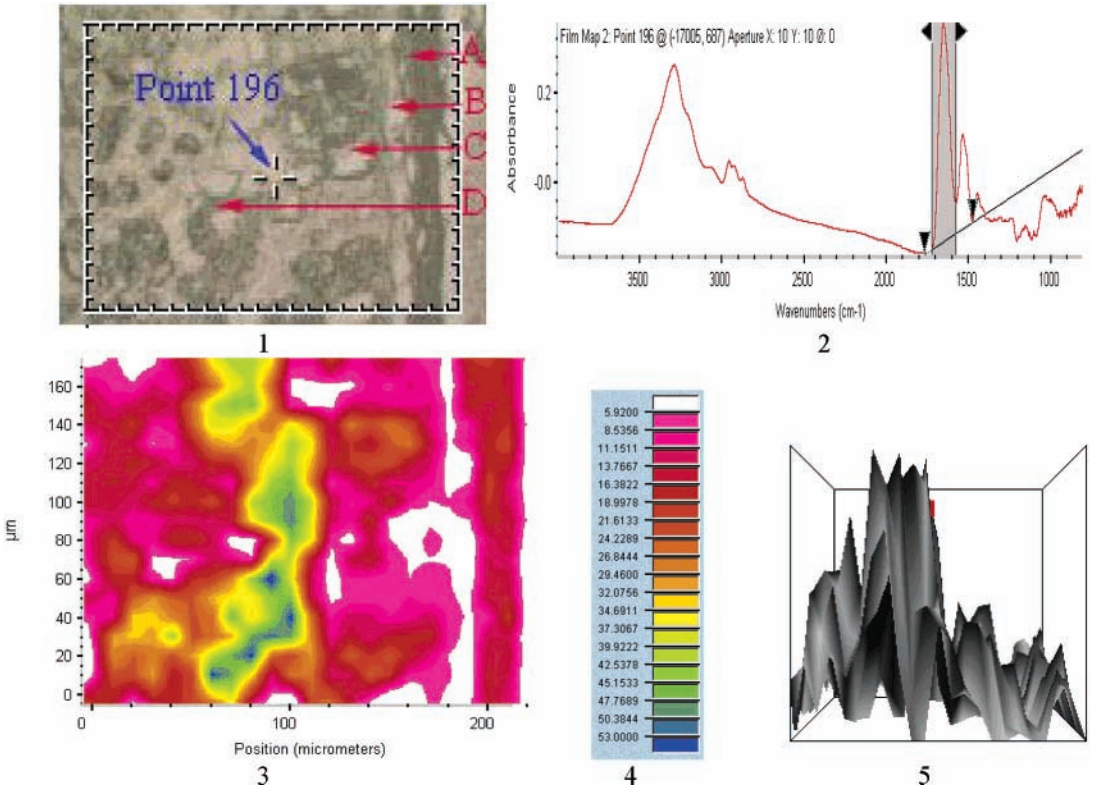

Figure 4. Area under 1650 cm^{-1} peak (amide I) showing protein distribution and concentration: (**1**) visible image [(**A**) pericarp; (**B**) seed coat; (**C**) aleurone; (**D**) endosperm region]; (**2**) spectrum corresponding to the pixel at the cross hair in the visible image; (**3**) chemical image; (**4**) chemical intensity ruler; (**5**) 3D image.

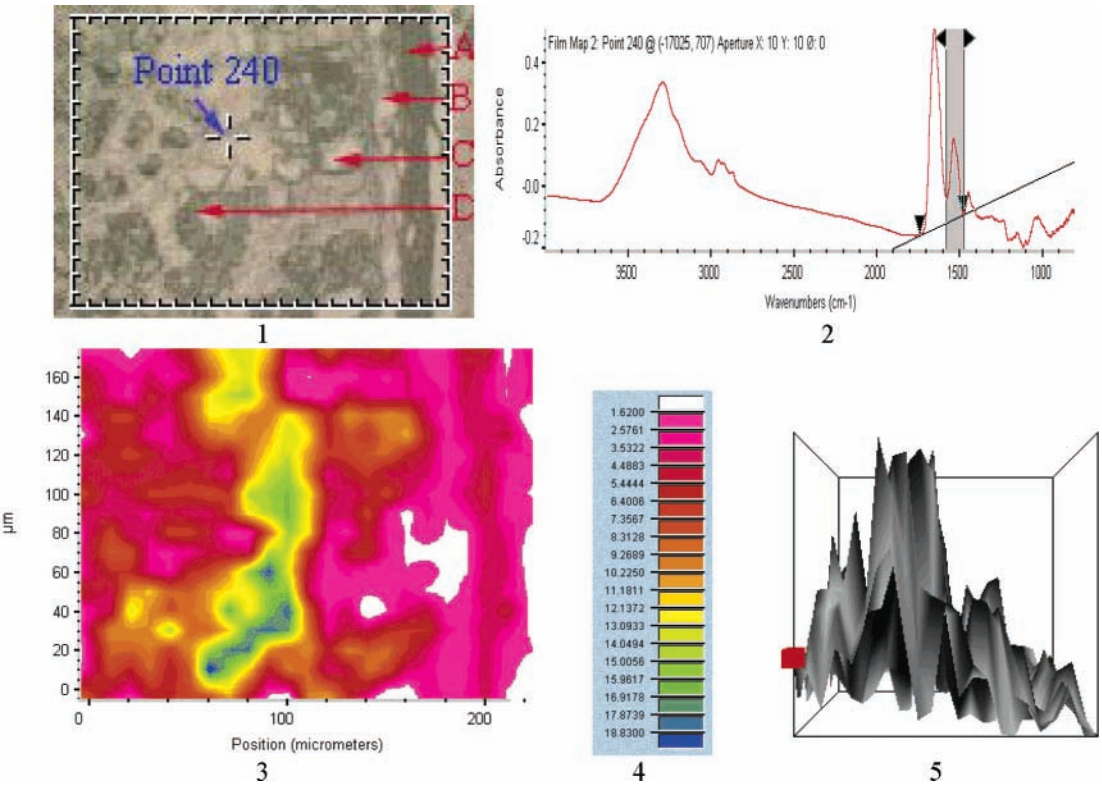

Figure 5. Area under 1550 cm^{-1} peak (amide II) showing protein distribution and concentration: (**1**) visible image [(**A**) pericarp; (**B**) seed coat; (**C**) aleurone; (**D**) endosperm region]; (**2**) spectrum corresponding to the pixel at the cross hair in the visible image; (**3**) chemical image; (**4**) chemical intensity ruler; (**5**) 3D image.

Ultraspatially Localized Chemical Analysis. *Distribution and Intensity of Biological Components.* It is widely known that IR spectroscopy has the ability to identify molecular constituents from their vibrational spectra (*9*). This so-called molecular fingerprint is found in the part of the IR spectrum often called the mid-IR region (*1*, *4*). A brief summary of the theory about

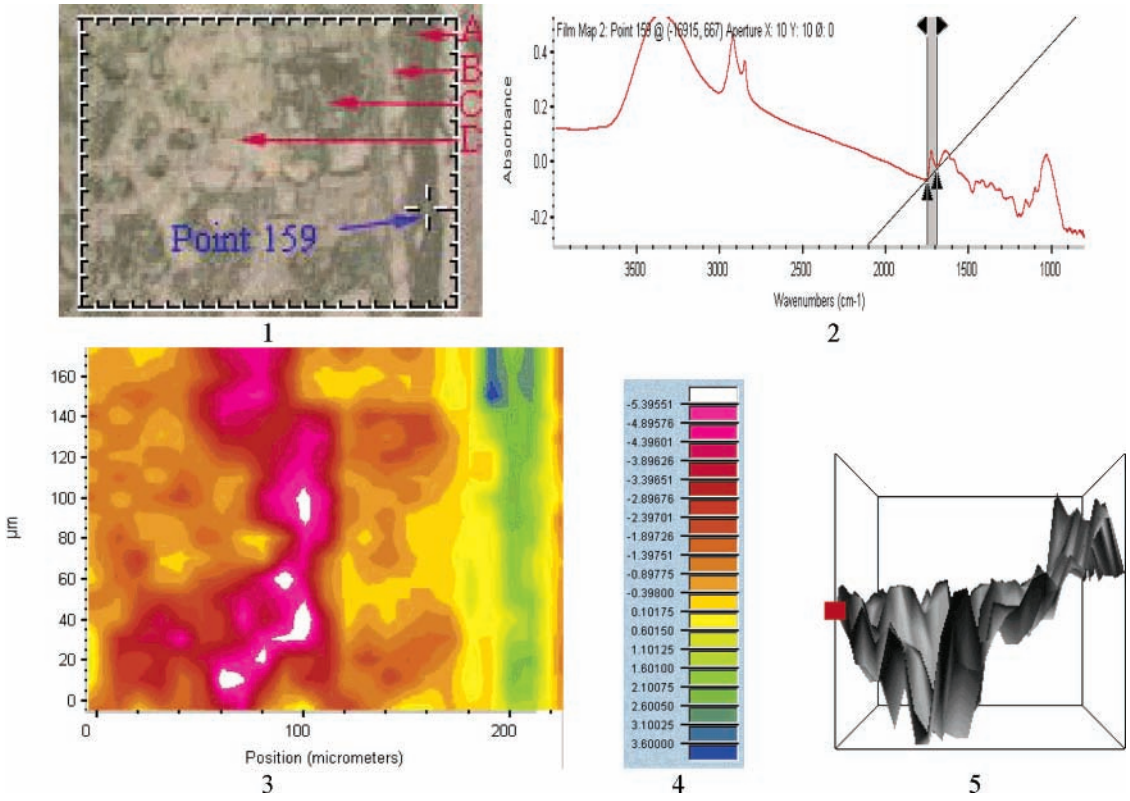

Figure 6. Area under peaks at 1738 cm^{-1} (carbonyl C═O ester linkage) showing lipid concentration and distribution: (**1**) visible image [(**A**) pericarp; (**B**) seed coat; (**C**) aleurone; (**D**) endosperm region]; (**2**) spectrum corresponding to the pixel at the cross hair in the visible image; (**3**) chemical image; (**4**) chemical intensity ruler; (**5**) 3D image.

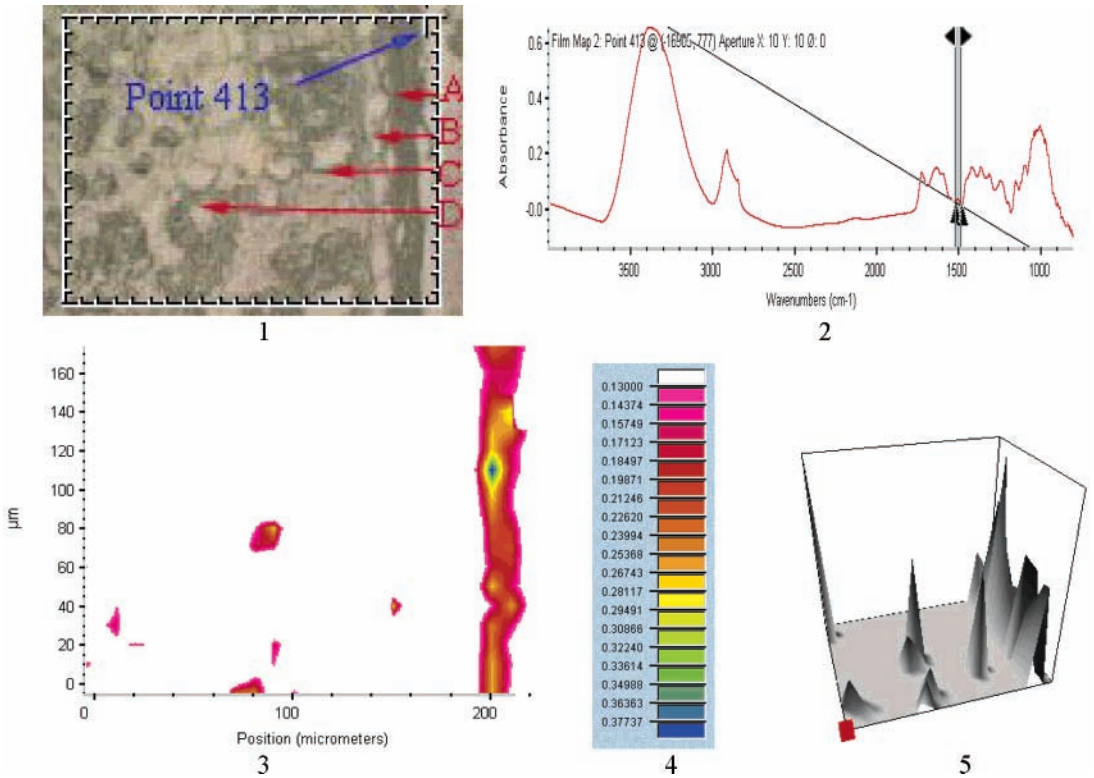

Figure 7. Area under peaks centered at 1510 cm^{-1} showing aromatic compounds, which indicate lignin concentration and distribution: (**1**) visible image [(**A**) pericarp; (**B**) seed coat; (**C**) aleurone; (**D**) endosperm region]; (**2**) spectrum corresponding to the pixel at the cross hair in the visible image; (**3**) chemical image; (**4**) chemical intensity ruler; (**5**) 3D image.

molecular energies, energy transitions, and IR radiation effect has been given in the Introduction (*7*−*10*). Within the mid-IR range, functional group assignments can be made from 4000 to ∼1300 cm^{-1}, allowing recognition of the presence of biological components (proteins, lipids, or aromatic compounds), and the region under 1300 cm^{-1}, known as the "fingerprint", allows

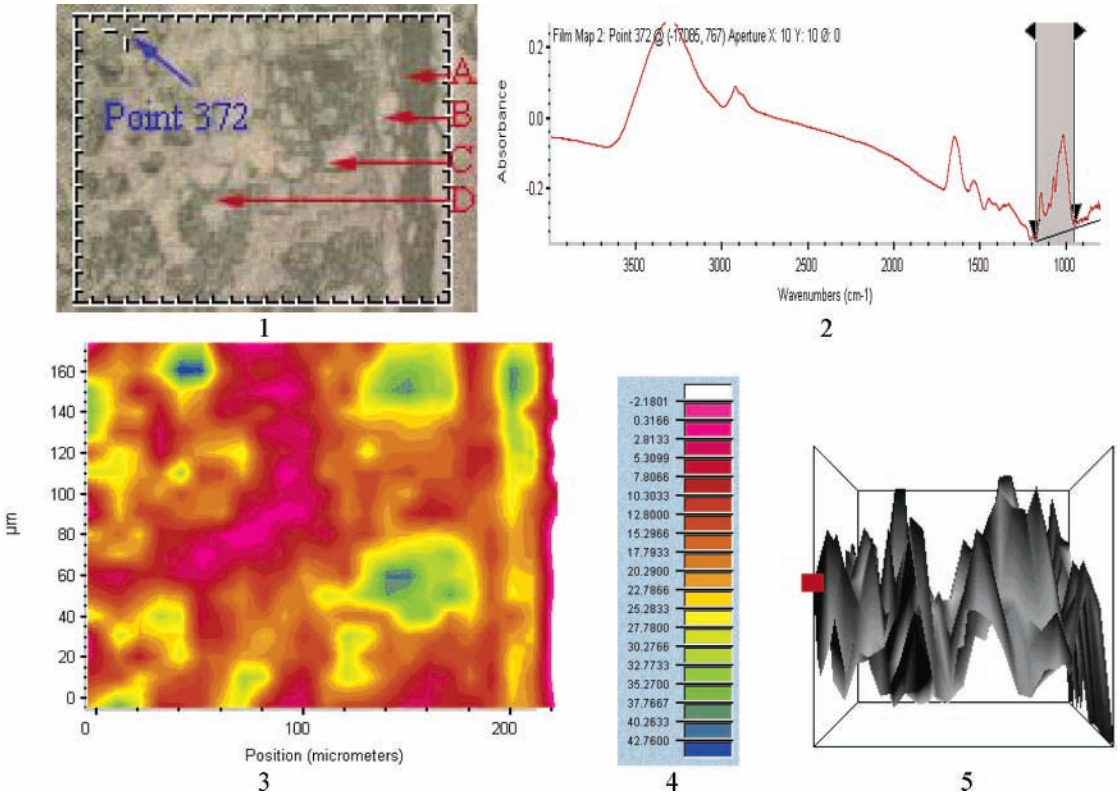

Figure 8. Area under peaks between 1180 and 950 cm^{-1} indicating total carbohydrates concentration and distribution: (**1**) visible image [(**A**) pericarp; (**B**) seed coat; (**C**) aleurone; (**D**) endosperm region]; (**2**) spectrum corresponding to the pixel at the cross hair in the visible image; (**3**) chemical image; (**4**) chemical intensity ruler; (**5**) 3D image.

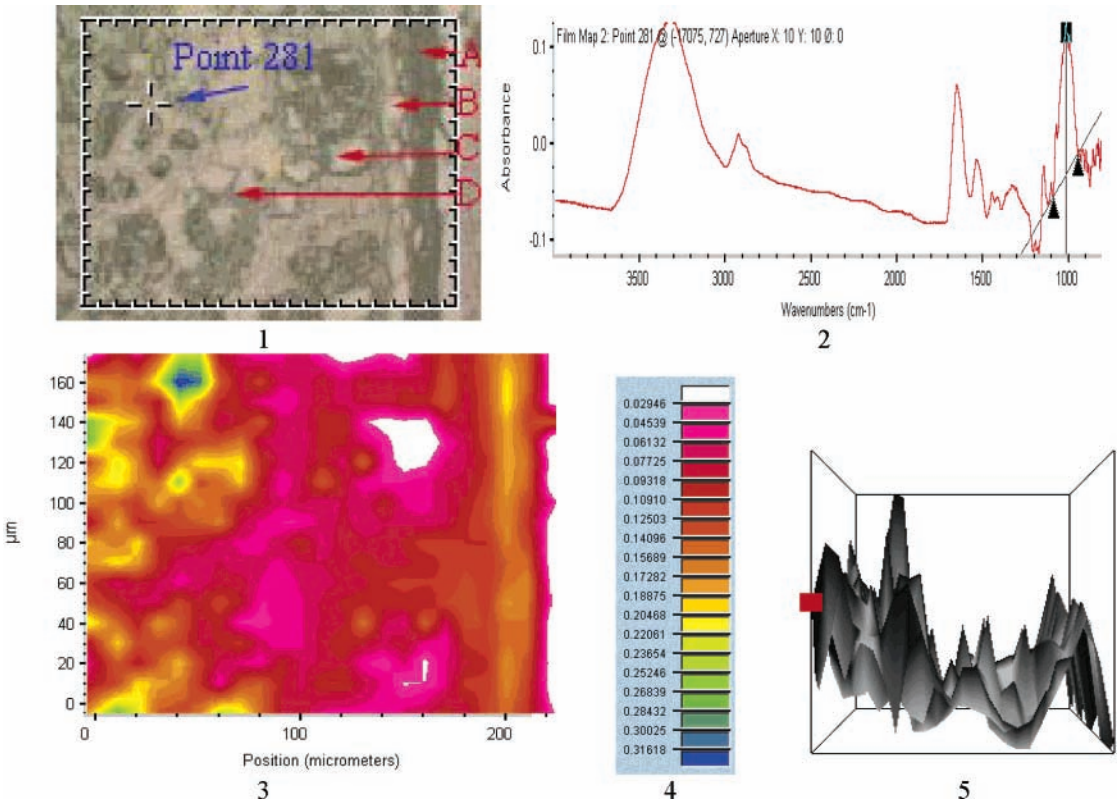

Figure 9. Height under peaks at 1025 cm^{-1} indicating nonstructural carbohydrates, mainly starch, concentration and distribution: (**1**) visible image [(**A**) pericarp; (**B**) seed coat; (**C**) aleurone; (**D**) endosperm region]; (**2**) spectrum corresponding to the pixel at the cross hair in the visible image; (**3**) chemical image; (**4**) chemical intensity ruler; (**5**) 3D image.

the eventual identification of a compound by comparison with spectra from known compounds.

In plant feed samples, the primary biological components include protein, lipid, lignin, and carbohydrates including structural and nonstructural carbohydrates (cellulose, hemicellulose, and starch), all of which have specific spectral features in the

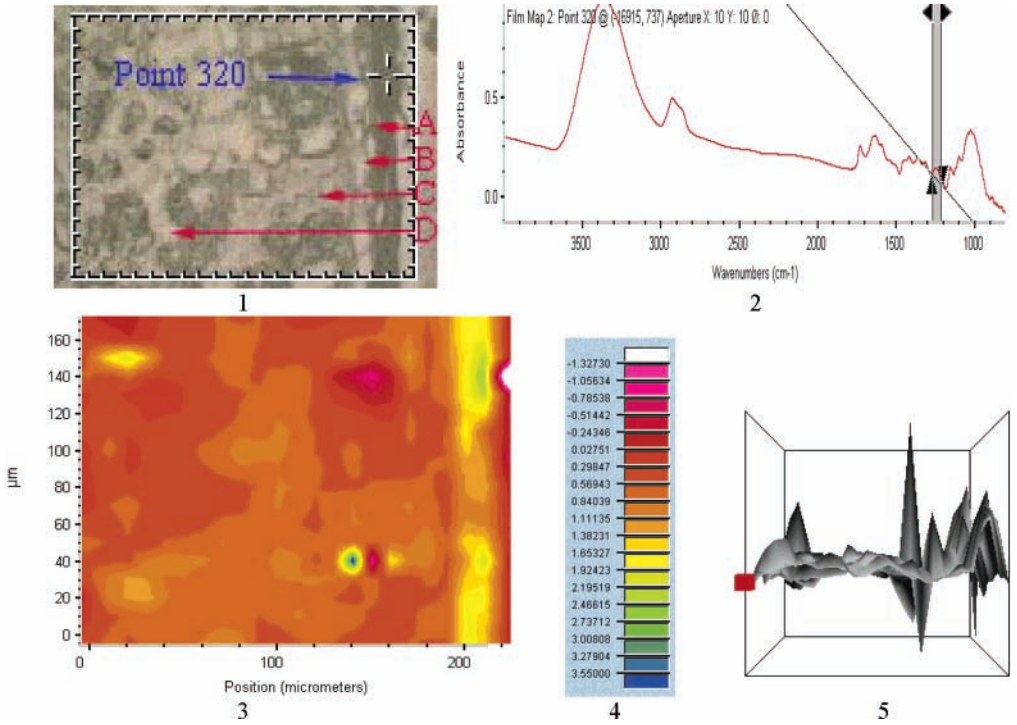

Figure 10. Area under peaks at 1246 cm^{-1} indicating hemicellulosic material concentration and distribution: (**1**) visible image [(**A**) pericarp; (**B**) seed coat; (**C**) aleurone; (**D**) endosperm region]; (**2**) spectrum corresponding to the pixel at the cross hair in the visible image; (**3**) chemical image; (**4**) chemical intensity ruler; (**5**) 3D image.

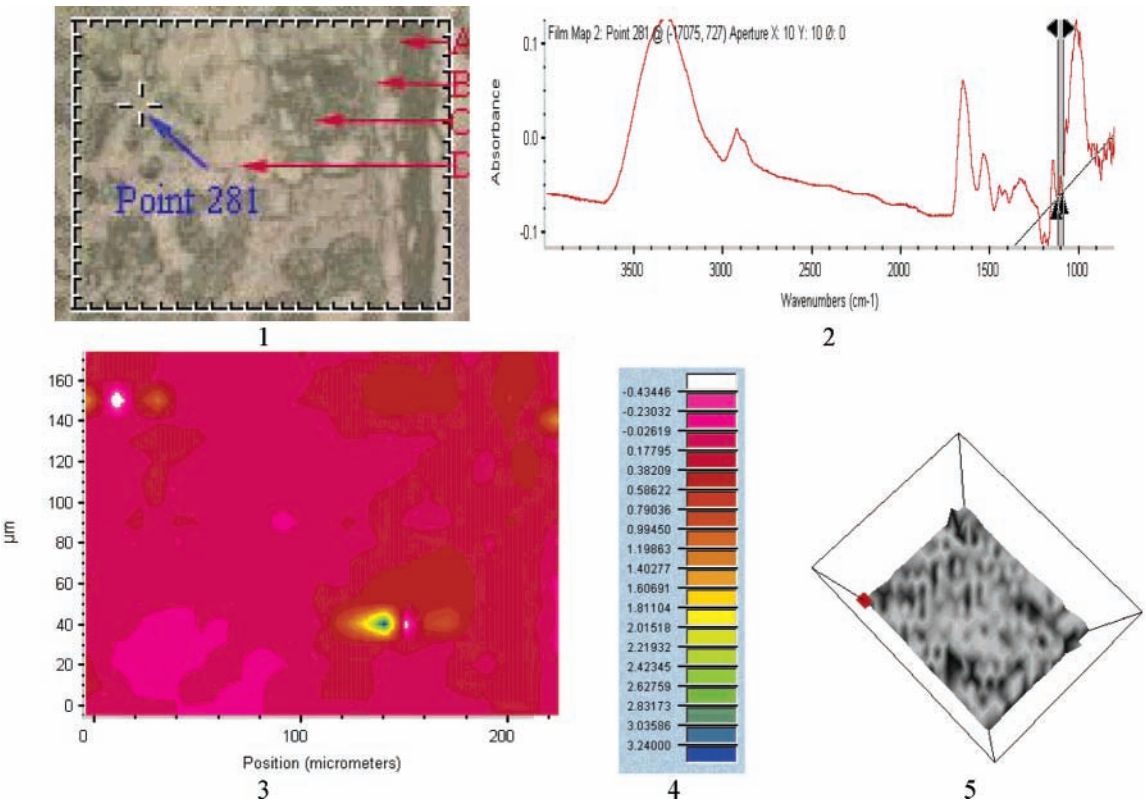

Figure 11. Area under peaks at 1100 cm^{-1} indicating cellulosic material concentration and distribution: (**1**) visible image [(**A**) pericarp; (**B**) seed coat; (**C**) aleurone; (**D**) endosperm region]; (**2**) spectrum corresponding to the pixel at the cross hair in the visible image; (**3**) chemical image; (**4**) chemical intensity ruler; (**5**) 3D image.

mid-IR region (*2*, *3*, *14*). The fingerprint bands of the functional groups, which indicate major biological components in plant feeds, are shown in **Figure 2** (*1*, *2*, *4*, *6*, *7*, *14*).

Figures 3−**11** represent color maps of functional groups of the grain barley tissue through the pericarp, seed coat, aleurone, and endosperm area and single-pixel spectra measuring an area as small as 10 × 10 μm of the sample. They show the distribution and relative concentration of the components

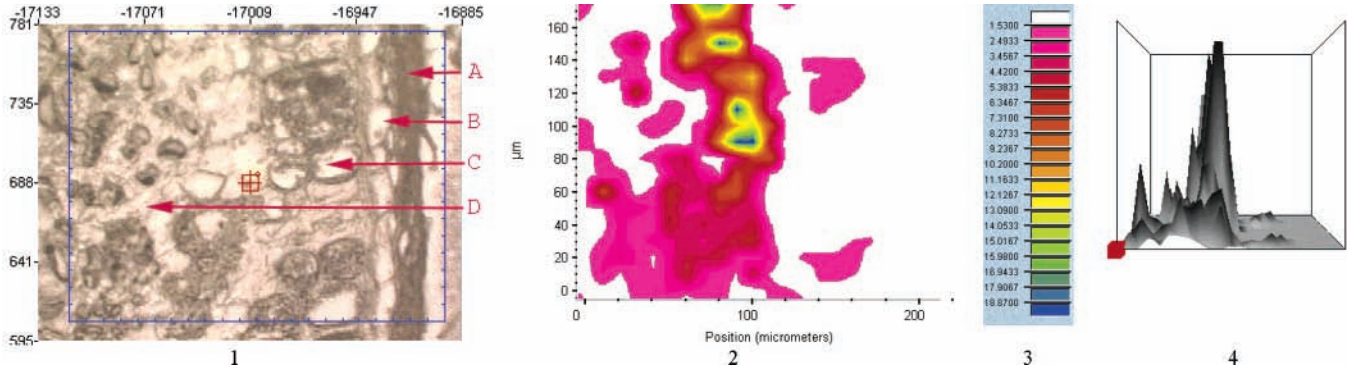

Figure 12. Peak height ratio representing protein to total starch ratio, obtained by the height under the 1650 cm^{-1} band divided by the height under the peaks 1025 cm^{-1} at each pixel: (**1**) visible bright field image of the mapped area outlined by the lined box, from pericarp (**A**), seed coat (**B**), aleurone (**C**), and endosperm area (**D**); (**2**) chemical image; (**3**) chemical intensity ruler; (**4**) 3D image.

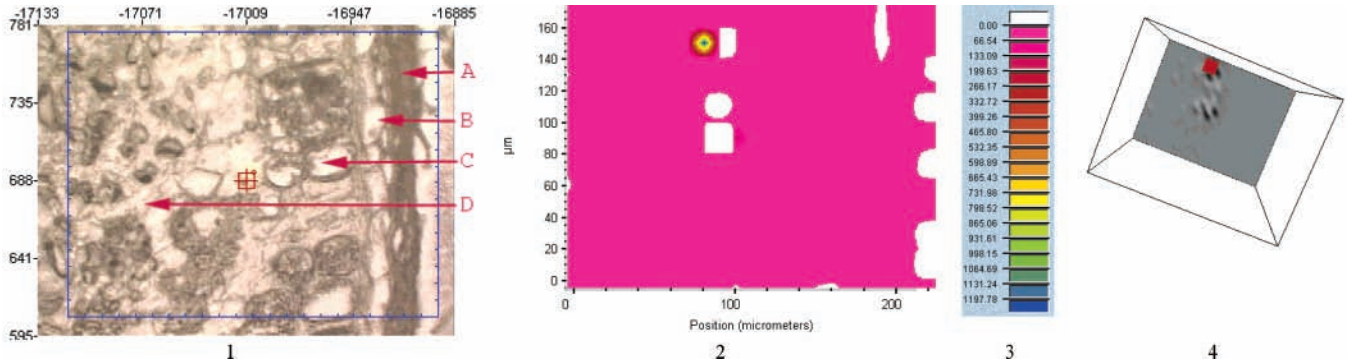

Figure 13. Peak area ratio representing protein to total carbohydrate ratio, obtained by the area under the 1650 cm^{-1} band divided by the area under the peaks between 1180 and 950 cm^{-1} at each pixel: (**1**) visible bright field image of the mapped area outlined by the lined box, from pericarp (**A**), seed coat (**B**), aleurone (**C**), and endosperm area (**D**); (**2**) chemical image; (**3**) chemical intensity ruler; (**4**) 3D image.

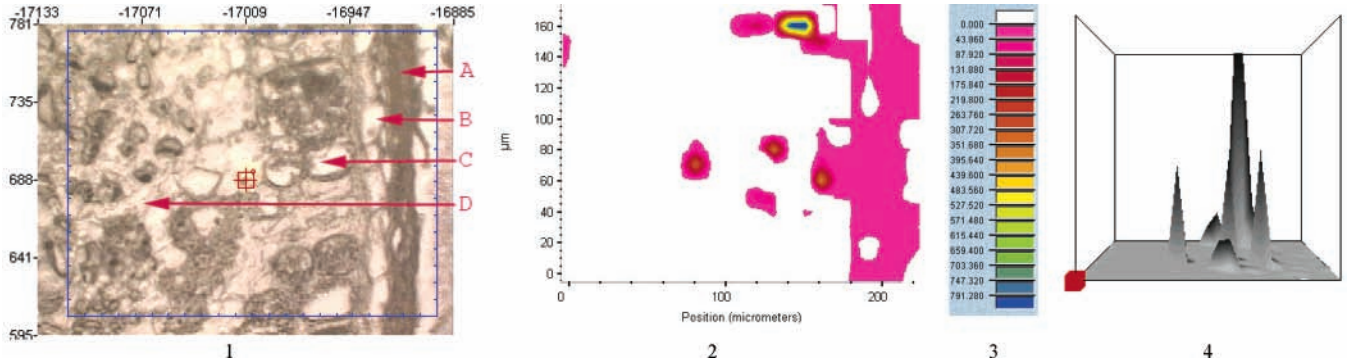

Figure 14. Peak height ratio representing protein to lipid ratio, obtained by the height under the 1650 cm^{-1} band divided by the height under the peaks 1738 cm^{-1} at each pixel: (**1**) visible bright field image of the mapped area outlined by the lined box, from pericarp (**A**), seed coat (**B**), aleurone (**C**), and endosperm area (**D**); (**2**) chemical image; (**3**) chemical intensity ruler; (**4**) 3D image.

associated with the plant inherent microstructure, imaged in false-color representation of chemical intensities. Blue stands for high intensity, red stands for low intensity, and white stands for no functional groups. The spectrum in each figure corresponds to the pixel in the cross hair and was selected to represent the value of the integrated peak. The represented spectra show a wide variety of spectral characteristics, which manifest the chemical composition in different morphological parts of the seed. **Figure 3** is the area under the full range 4000 to 800 cm^{-1} peak showing mid-IR total functional groups intensity in the tissue.

Figures 4 and **5** show the areas under the 1650 cm^{-1} peak attributed to protein amide I absorption and under the 1550 cm^{-1} peak attributed to protein amide II absorption (*1*, *5*). The amide I (1650 cm^{-1}) and amide II (1550 cm^{-1}) are characteristics of C═O and N−H bonds in the protein backbone and are indicators of the area of the sample where protein is present (*1*, *4*, *6*). Both figures show that proteins are unequally distributed and lower in the pericarp and seed coat region and higher in subendosperm areas.

Figure 6 shows the areas under the 1738 cm^{-1} peak. The band at 1738 cm^{-1} is due to the carbonyl group (C═O) stretching vibration in the ester linkage (*1*, *4*, *6*), which indicates the lipid distribution and concentration. The results show higher lipids in the pericarp region.

Figure 7 shows the areas under 1510 cm^{-1}. The 1510 cm^{-1} band corresponds to the stretch associated with para-substituted benzene rings and can be associated with aromatic species present only in the tissue (*1*, *3*, *13*). The lignin band originates from the aromatic signals (*7*, *8*, *13*). The results show that only the pericarp region contained higher aromatic compounds, although the intensity of the aromatic compound was low.

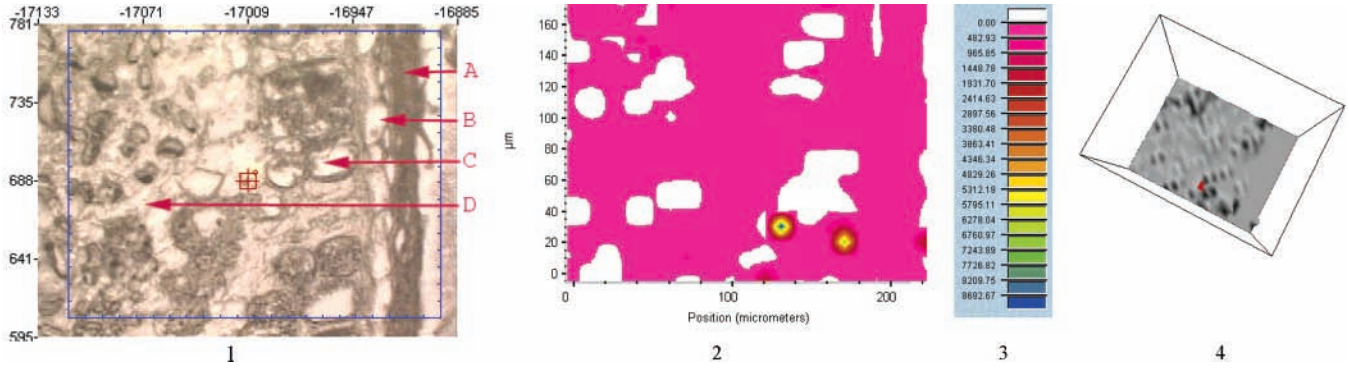

Figure 15. Peak height ratio representing protein to lignin ratio, obtained by the height under the 1650 cm^{-1} band divided by the height under the peaks 1510 cm^{-1} at each pixel: (1) visible bright field image of the mapped area outlined by the lined box, from pericarp (**A**), seed coat (**B**), aleurone (**C**), and endosperm area (**D**); (**2**) chemical image; (**3**) chemical intensity ruler; (**4**) 3D image.

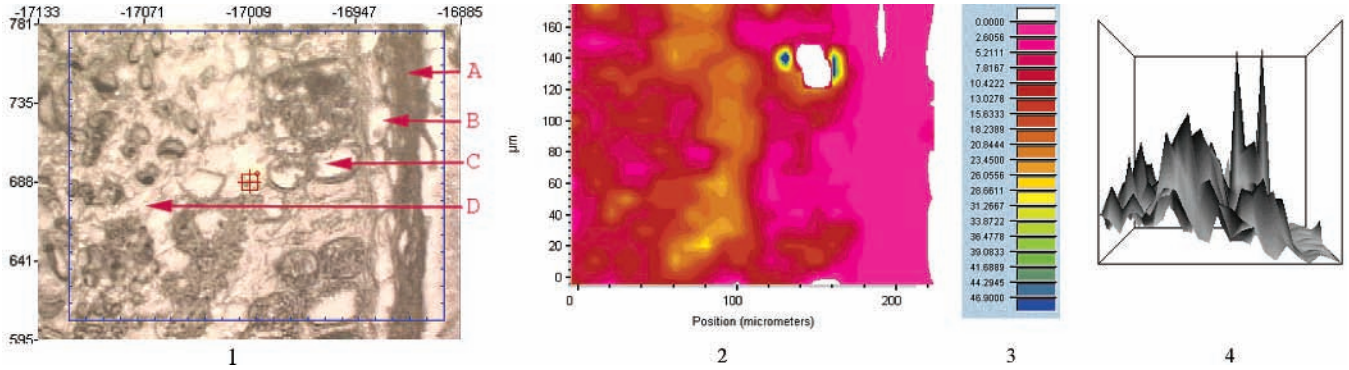

Figure 16. Peak height ratio representing protein to hemicellulose ratio, obtained by the height under the 1650 cm^{-1} band divided by the height under the peaks 1246 cm^{-1} at each pixel: (**1**) visible bright field image of the mapped area outlined by the lined box, from pericarp (**A**), seed coat (**B**), aleurone (**C**), and endosperm area (**D**); (**2**) chemical image; (**3**) chemical intensity ruler; (**4**) 3D image.

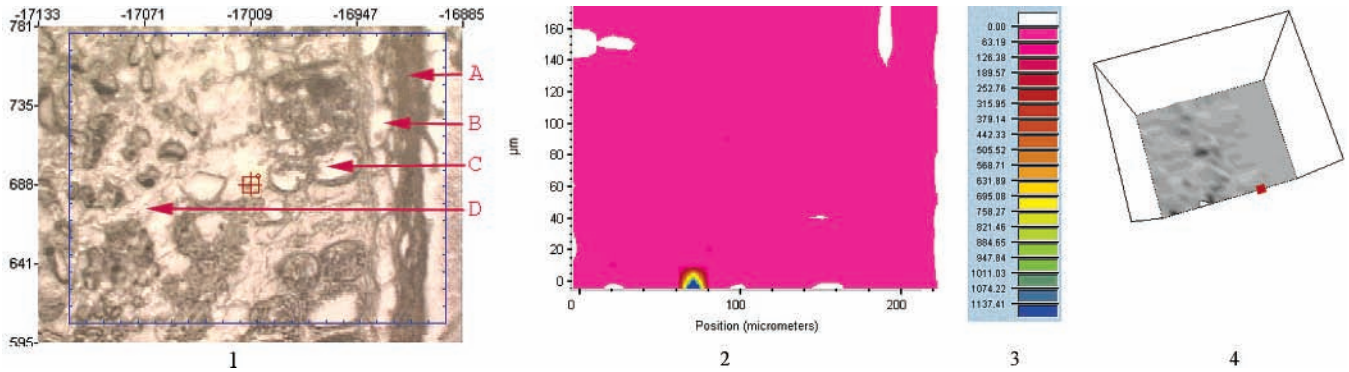

Figure 17. Peak height ratio representing protein to cellulose ratio, obtained by the height under the 1650 cm^{-1} band divided by the height under the peaks 1100 cm^{-1} at each pixel: (**1**) visible bright field image of the mapped area outlined by the lined box, from pericarp (**A**), seed coat (**B**), aleurone (**C**), and endosperm area (**D**); (**2**) chemical image; (**3**) chemical intensity ruler; (**4**) 3D image.

Carbohydrates consist of sugars with numerous OH and CO bonds. Depending on bond linkage and type of sugars, the IR position for carbohydrate is between 1180 and 950 cm^{-1}. The area under the peaks between 1180 and 950 cm^{-1} is plotted in **Figure 8**; it indicates total carbohydrate absorption, including structural and nonstructural carbohydrates. The results show the carbohydrates are unequally distributed. **Figure 9** shows the height under the 1025 cm^{-1} peak, which mainly indicates starch spatial distribution and intensity (*3*, *7*, *14*). The results show higher contents in the endosperm region. **Figures 10** and **11** show the area under the 1246 and 1100 cm^{-1} peaks, which indicate hemicellulose and cellulose spatial distribution and intensities. The results show a higher content of hemicellulose in the pericarp region.

Ratios of the Biological Components. Different biological component ratio images in the tissue (e.g., protein to total starch ratio image; hemicellulose to total carbohydrate ratio image), showing structural chemical features, can be obtained by the height or area under one functional group band (e.g., amide I, 1650 cm^{-1}) divided by the height or area under another functional group band (e.g., starch, 1025 cm^{-1}) at each pixel (pixel size = 10 × 10 μm). **Figures 12**−**19** are peak ratio maps, representing biological component ratio distribution and intensity in the inherent structure. The area or height under the 1650 cm^{-1} band divided by the area or height under the peaks around 1025 cm^{-1}, between 1180 and 1000 cm^{-1}, and at 1738, 1510, 1246, and 1100 cm^{-1}, at each pixel, represent protein to total starch (**Figure 12**), total carbohydrates (**Figure 13**), lipid (**Figure 14**), lignin (**Figure 15**), hemicellulose (**Figure 16**), and cellulose ratios (**Figure 17**) in the tissue, respectively. They clearly show

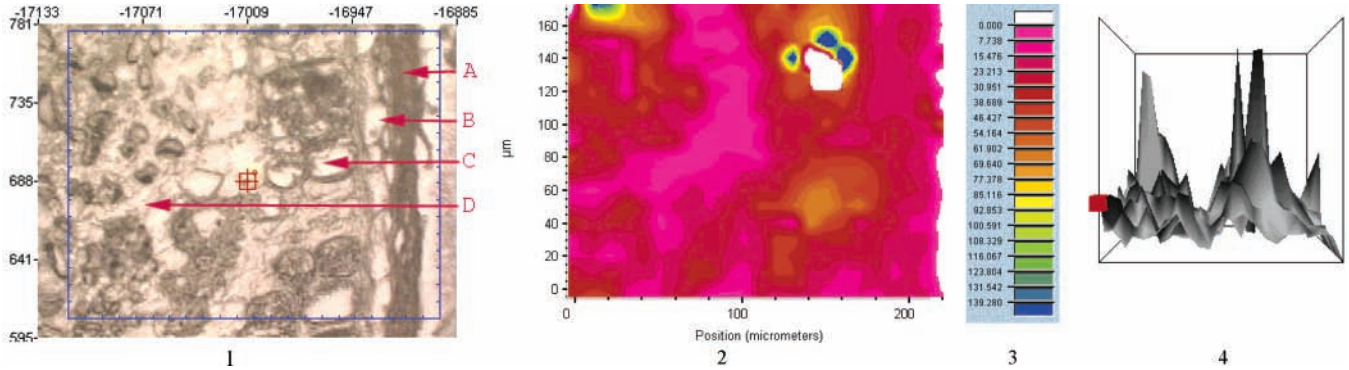

Figure 18. Peak area ratio representing total carbohydrate to hemicellulose ratio, obtained by area under the peaks between 1180 and 950 cm^{-1} divided by the area under the peak 1246 cm^{-1} at each pixel: (**1**) visible bright field image of the mapped area outlined by the lined box, from pericarp (**A**), seed coat (**B**), aleurone (**C**), and endosperm area (**D**); (**2**) chemical image; (**3**) chemical intensity ruler; (**4**) 3D image.

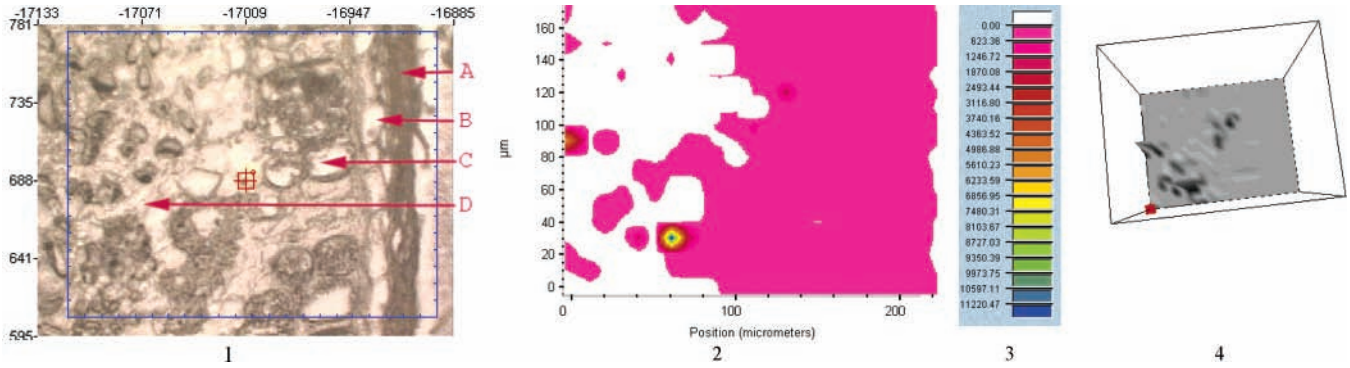

Figure 19. Peak area ratio representing total carbohydrate to cellulose ratio, obtained by area under the peaks between 1180 and 950 cm^{-1} band divided by the area under the peaks 1100 cm^{-1} at each pixel: (1) visible bright field image of the mapped area outlined by the lined box, from pericarp (**A**), seed coat (**B**), aleurone (**C**), and endosperm area (**D**); (**2**) chemical image; (**3**) chemical intensity ruler; (**4**) 3D image.

biological component ratio distributions and intensities. The area under the peaks between the 1180 and 950 cm^{-1} bands divided by the area under the peaks at 1246 and 1100 cm^{-1} at each pixel represent total carbohydrate to hemicellulose (**Figure 18**) or cellulsose ratios (**Figure 19**) in the tissue, respectively (**Figures 18** and **19**).

Such biological component ratio mapping or imaging has two advantages. The first is that, using those ratios, any spectral intensity variations due to tissue thickness changes are eliminated. The second is that the ratio maps are able to indicate relative biological component contents, which could be used to determine food or feed quality characteristics, and nutritive values and for use in plant-breeding programs. Ratio mapping can be used to compare different barley varieties according to the inherent structural spectral characteristics, chemical functional group intensity, and distribution (e.g., seed coat features, pericarp features between different varieties of barley). It can be used to chemically define the plant feed intrinsic structure and analyze individual plant structure with intact tissue.

In conclusion, synchrotron transmission FTIR microspectroscopy could be used as a rapid, direct, and nondestructive analytical technique to reveal molecular microstructural–chemical features within the tissue in grain barley, in terms of spectral, functional group, and biological component characteristics and ratios. Such information and analytical technique can be used for plant-breeding programs for selecting superior varieties of barley for special purposes. The localized structural–chemical information obtained from this technique could also be used to predict barley quality and nutritive value for humans and animals.

ACKNOWLEDGMENT

We are grateful to Drs. N. S. Marinkovic and L. M. Miller (NSLS-BNL, Upton, NY) for helpful discussion and data collection at the U10B synchrotron station and Dr. Brain G. Rossnagel, Crop Development Center, University of Saskatchewan, for providing barely samples.

LITERATURE CITED

(1) Wetzel, D. L. When molecular causes of wheat quality are known, molecular methods will supersede traditional methods. *Proceedings of the International Wheat Quality Conference II*, Manhattan, KS, May 2001; pp 1–20.

(2) Miller, L. M.; Carlson, C. S.; Carr, G. L.; Chance, M. R. A Method for Examining the Chemical Basis for Bone Disease: Synchrotron Infrared Microspectroscopy. *Cell. Mol. Biol. (Paris)* **1998**, *44*, 117–127.

(3) Wetzel, D. L.; Eilert, A. J.; Pietrzak, L. N.; Miller, S. S.; Sweat, J. A. Ultraspatially resolved synchrotron infrared microspectroscopy of plant tissue in situ. *Cell. Mol. Biol. (Paris)* **1998**, *44*, 145–167.

(4) Marinkovic, N. S.; Huang, R.; Bromberg, P.; Sullivan, M.; Toomey, J.; Miller, L. M.; Sperber, E.; Moshe, S.; Jones, K. W.; Chouparova, E.; Lappi, S.; Franzen S.; Chance, M. R. Center for Synchrotron Biosciences' U2B beamline: an international resource for biological infrared spectroscopy. *J. Synchrotron Radiat.* **2002**, *9*, 189–197.

(5) Miller, L. M. The impact of infrared synchrotron radiation on biology: past, present, and future. *Synchrotron Radiat. News* **2000**, *13*, 31–37.

(6) Miller, L. M. Infrared Microsperctroscopy and Imaging; http://nslsweb.nsls.bnl.gov/nsls/pubs/nslspubs/imaging0502/irxrayworkshopintroduction.ht, accessed Oct 2002.

(7) Yu, P.; McKinnon, J. J.; Christensen, C. R.; Christensen, D. A. Mapping Plant Composition with Synchrotron Infrared Microspectroscopy and Relation to Animal Nutrient Utilization. *Proceedings of The Canadian Society of Animal Science−2003 Conference*, University of Saskatchewan, Saskatoon, SK, Canada, June 10−13, 2003; pp 1−20 (Invited Article and Conference Speech).

(8) Hergert, H. L. *Infrared Spectra, Lignins: Occurrence, Formation, Structure and Reactions*; Sarkanen, K. V., Ludwig, C. H., Eds.; Wiley-Interscience: New York, 1971.

(9) Joe, L. W.; Roth, C. B. *Infrared Spectrometry, Method of Soil Analysis, Part 1. Physical and Mineralogical Methods*, 2nd ed.; Agronomy Monograph 9; Amercian Society of Agronomy−Soil Science Society of America: Madison, WI, 1986.

(10) Mathlouthi, M.; Koenig, J. L. Vibrational Spectra of Carbohydrates. *Adv. Carbohydr. Chem. Biochem.* **1986**, *44*, 7−89.

(11) Kemp, W. *Organic Spectroscopy*, 3rd ed.; Freeman: New York, 1991.

(12) Michael, J.; Mantsch, H. H. Biomedical Infrared Spectroscopy. In *Infrared Spectroscopy of Biomolecules*; Mantsch, H. H., Chapman, D., Eds.; Wiley-Liss: New York, 1996; pp 311−340.

(13) Himmelsbach, D. S.; Khalili, S.; Akin, D. E. FT-IR microspectroscopic imaging of flax (*Linum usitatissimum* L.) stems. *Cell. Mol. Biol. (Paris)* **1998**, *44*, 99−108.

(14) Yu, P.; McKinnon, J. J.; Christensen, C. R.; Christensen, D. A.; Marinkovic, N. S.; Miller, L. M. Chemical imaging of microstructures of plant tissues within cellular dimension using synchrotron infrared microspectroscopy. *J. Agric. Food Chem.* **2003**, *51*, 6062−6067.

(15) Yu, P.; Christensen, D. A.; Christensen, C. R.; Drew, M. D.; Rossnagel, B. G.; McKinnon, J. J. Use of synchrotron Fourier transform infrared microspectroscopy to identify chemical differences in the ultrastructural matrix of endosperm tissue between Harrington (malting-type) and Valier (feed-type) barley in relation to rumen degradation characteristics. *Can. J. Anim. Sci.* **2004**, in press.

(16) Yu, P.; Meier, J.; Christensen, D. A.; Rossnagel, B. G.; McKinnon, J. J. Using the NRC-2001 model and the DVE/OEB system to evaluate nutritive values of Harrington (malting-type) and Valier (feed-type) barley for ruminants. *Anim. Feed Sci. Technol.* **2003**, *107*, 45−60.

Received for review September 18, 2003. Revised manuscript received January 6, 2004. Accepted January 17, 2004. The National Synchrotron Light Source in Brookhaven National Laboratory (NSLS-BNL, Upton, NY) is supported by U.S. Department of Energy Contract DE-AC02-98CH10886. This research has been supported by grants from the Saskatchewan Agricultural Development Fund (ADF).

JF035065A